Biologic tissues properties deduction using an opto-mechanical model of the human eye

A.V. Maurer[1], D.P. Enfrun[2], C.O. Zuber[3], R. Rozsnyo[4]
1. R&D, Kejako, Plan-les-ouates, GE, Switzerland
2. R&D, Kejako, Plan-les-ouates, GE, Switzerland
3. R&D, Kejako, Plan-les-ouates, GE, Switzerland
4. MNCM, HES-SO, Geneva, GE, Switzerland

Abstract

The visual accommodation is a complex biomechanical & optical process. Today in vivo imaging technologies do not allow to measure the eye components material properties such as the refractive index or the stiffness: these properties are essential to understand & diagnose the effect of aging on the eye accommodative performance and develop new surgeries. To address this problem, Kejako has set up a parametric 3D mechanical model of the human eye, in addition with an optical evaluation.

This paper present how this model can be used to deduce with reverse engineering some of these non-measurable properties from in vivo imaging such as the refractive index distribution in the Crystalline Lens. Furthermore, we will open the discussion on some potential application of this model for Presbyopia or other eye disorders.

KEYWORDS: Biomechanics, Optics, Imaging, Reverse Engineering, Human Vision, GRIN, Refractive Index, Soft Tissues

---

I. Introduction

Mechanism of the human eye accommodation and aging

The eye is composed of several main organs **[Figure 1]**. First the cornea, a transparent fibrous tissue that interfaces the air and the inside of the eye. The cornea is linked to the sclera, an opaque and relatively rigid white tissue that enables the structure of the whole eye. The iris acts as a diaphragm, and is tied to the ciliary muscle. This complex ring-like muscle is connected to the sclera through the posterior zonula, and to the lens through the lens zonula. The zonula is a web of suspensory stiff ligaments.
The crystalline lens is a soft ellipsoidal transparent tissue whose deformations enable changes of focus on the retina.
The space between the crystalline lens and the cornea is filled with a liquid called the aqueous humor, and the back of the eye is filled with a jelly tissue called the vitreous body.

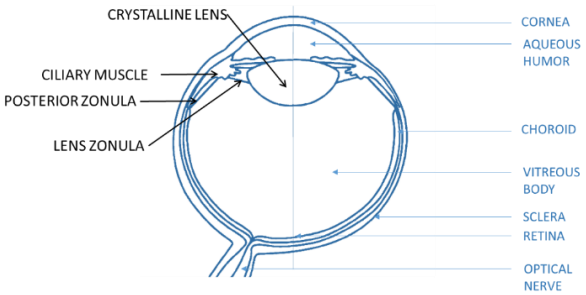

Figure 1: Anatomy of the human eye, on the left *(black arrow)* the organs mainly involved in the accommodation process, on the right *(blue arrow)* the other organs of the eye **[3]**

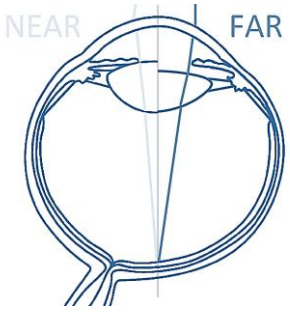

Figure 2: The light trajectory through the eye for different distance of vision

The light coming from an object enters the eye via the cornea, propagates in the aqueous humor, the crystalline lens and the vitreous body, until it reaches the retina, a surface made of photoreceptors that will convert light into neuronal impulsions to the brain **[Figure 2]**.
The young emmetropic human sight can naturally adapt its distance of focus for far and near objects: this is called *the accommodation process* and consists of several factors such as pupil constriction, eye convergence, brain processing, and among all a change of the crystalline lens shape due to a biomechanical effort **[4]**.

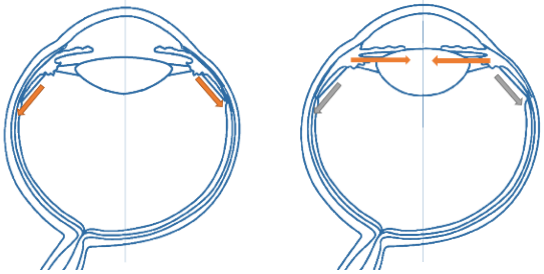

Figure 3: a) *Left*, the passive tension in the posterior zonula *(orange)* flattens the crystalline lens for far vision. **b).** *Right*, the active constriction of the ciliary muscle *(orange)* enables the lens to go back to its natural shape by countering the permanent tension stored in the posterior zonula *(grey)*

The biomechanical process under these changes of the crystalline lens power may be disconcerting, because the resting state of vision (far vision) correspond to the most mechanically stressed configuration of the lens (*flattened*), but the efforts for focusing on near vision correspond to the lowest stress in the lens. The far vision is thus passive, and the near vision active.
Here is how it works: the lens is permanently submitted to an equatorial stretching tension stored in the posterior zonula, going through the ciliary muscle and transmitted by the lens zonula - *a web-like ring that links the ciliary muscle and the sclera with the lens*. The posterior zonula acts as a spring, and the ciliary muscle being inactive, all the tension stored in the zonula is transmitted to the lens that flattens, enabling a focus for far vision **[Figure 3.a.]**. When the ciliary muscle contracts, its movement enable the lens to go back to its stress free round shape, to focus on closer objects **[Figure 3.b.]**.

While aging, geometric changes happen mostly in the lens. Its growth pulls the ciliary ring forward, and the lens material properties progressively get stiffer **[Figure 4.a]**: the whole compliance of the lens is affected until there's almost no amplitude of deformation **[Figure 4.b]**. The refractive index of the lens and its distribution drop **[5]**, and the most accommodated shape tends to become the far vision. This age-related loss of the near vision is called presbyopia.

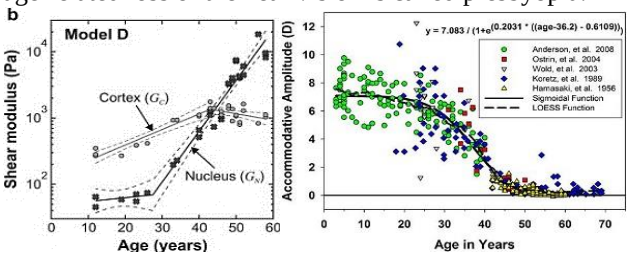

Figure 4 : a) *Left* : Change in the lens mechanical properties with age from Wilde & Al. **[1] b)** *Right* : Objective measurement of accommodation amplitude with age from Anderson & Al. **[2]**

Finite element modelling and accommodation

Numerical simulation of the accommodation has been studied since the early 80-90's with a first focus on the interaction between accommodation, vergence and pupillary constriction and the corresponding phasic and tonic responses. Starting from a static systemic representation of the eye, models have evolved towards dynamic systemic representation. **[12]** During the beginning of the early 21st century with the growth of numerical computing power, 2D and 3D models of the eye have been developed to improve the understanding of the accommodation process. Those models were either focusing on the mechanical aspects **[14] [17] [20]** or optical aspects **[15] [18]** of the accommodation. Therefore, only a few components were modelled (for instance mainly the lens, sometimes zonulas and/or vitreous body). Material properties of the elements of the eye such as the lens or the vitreous body were approximated with linear elasticity which did not take in account the real behavior of those soft tissues. More recently new models have been realized in which both mechanical and optical aspects are studied **[16] [19] [21]** with the two later ones being more complete 3D models. Those models try to go further in depth in order to catch the interaction between the mechanical and the optical aspects (separately evaluated). The modelling of the eye's components is a bit more complete with the presence of other eye components, but still a lot of simplifications were made.

In Vivo Characterisation of the eye

Today in vivo imaging technologies for ophthalmology are diverse, but none of them ensure complete practical clinical measurements. MRI *(Magnetic Resonance Imaging)* for instance, provides the best results when looking at the internal geometry with a low amount of distortion, but due to the size of the eye ball, its proximity with the brain, the spatial resolution and exposure time relationship makes it hard to use out of labs. OCT (*Optical Coherence Tomography*) enables to get information essentially on the optical axis (from cornea to retina), but induces some distortions. The UBM (*Ultrasound Bio-Microscopy*) enables imaging of non-transparent parts such as the ciliary muscle or the sclera, but induces high distortions. The Slit-lamp only enables imaging of the anterior segment (Cornea, lens) but provides good information about the lens shape after correction **[5] [6]**.
Due to these limitations, most of the in vivo imaging of the eye must be corrected and extrapolated. Moreover, the in vivo measurements of some material properties such has the stiffness (for UBM correction) or the refractive index (for OCT correction) remains difficult.

II. Material & Methods:

Parametric Complete model of the human eye

FEM models of the human eye are useful tools for developing innovative treatment and surgeries. Most of the material properties and the geometries are critical to develop a realistic modelling of the human eye accommodation.

A complete 3D *non-axisymmetric* model of the human eye accommodation has been developed and validated previously by our team. This model comprises all the main organs of the human eye involved in the accommodation process *(Cornea, Sclera, Iris, Ciliary Muscle, Zonular fibers, Lens capsule, Lens cortex, Lens Nucleus, Aqueous humor, Vitreous Body, Retina – see Figure 1 for anatomy)* using the **COMSOL *Non-Linear Structural Mechanics*** and ***Ray Optics*** **Modules** to ensure an opto-mechanical direct coupling.

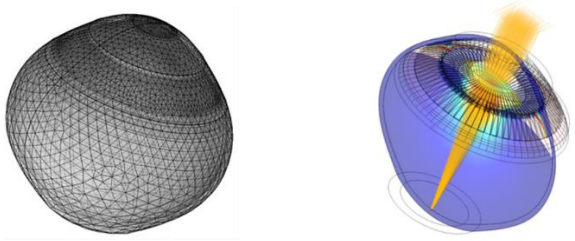

Figure 5: Opto-mechanical parametric model of the human eye developed by Kejako SA.

The geometry of the eye is fully parametric and generated by an external CAD software to adapt any measurable eye geometry. The 3D models also take into account the non axi-symmetry of the eye around the optical axis to model crystalline lens or corneal astigmatism. The geometries generated from statistics or measurement using OCT **[Figure 6]** were imported using the **CAD Import Module**.

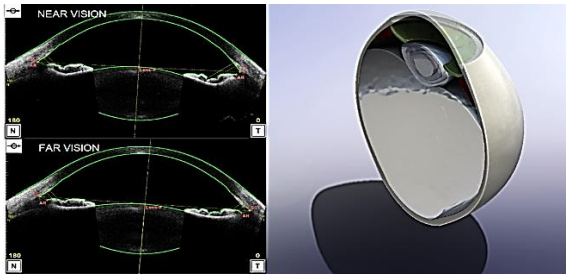

Figure 6: *Left:* OCT imaging of a young emmetropic female subject using the CASIA II *(Tomey). Right:* 3D Textured render of the subject's eye from OCT in the CAD Software

On the contrary to most models of the literature that only focus on an axi-symmetric modelling of the lens, the mechanical modelling includes all the essential organs of the human eye, and all the stakeholders involved directly or indirectly in the accommodation process. The model has been validated with in vivo imaging of patient's geometries and statistical databases.

The model was proven previously to be able to simulate entirely the presbyopia progression – i.e. the progressive loss of vision with aging - when applying the age-related geometric and material changes.

The optical results of the ray tracing were evaluated using the **Ray Optics module**. The central part of the retina was modelled with concentric subdivision corresponding to the optical resolution of the human eye. Theses subdivision were all associated with optical walls having accumulative light deposit properties.

The more the rays stop at the center of the retina, the more the value of the integrative score-function characterizing the acuity increases. This score can be displayed against other parameters to find a refractive index distribution or the distance of an object producing the best focus **[Figure 7]**.

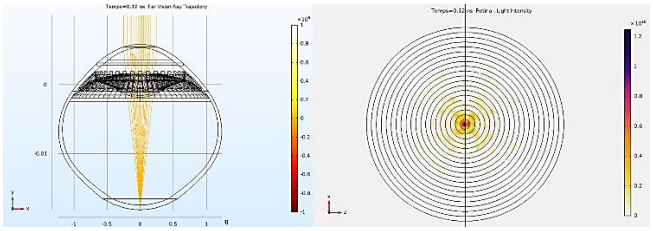

Figure 7: Ray tracing (left) and modeling of the central retinal resolution with concentric fine subdivision (right) with light deposit

The refraction of the lens can be set using a homogenous refractive index or spatial-dependent law. Using the **Wall distance physics**, and by associating the value of the refractive index to both the distance field generated and displacements, we have created a repartition of the refractive index that follows the deformation of the lens during accommodation. The shape of the law was obtained from the literature **[7] [Figure 8]**

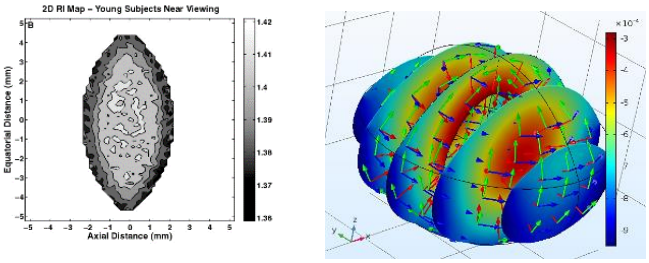

Figure 8.a: *(left)* Example of a gradient of refractive index measured with MRI from **[7]** **(***right)* 3D cuts of the distance gradient generated with wall distance physic. A mathematic function **[Equation 1]** can be applied to this distance field to convert it in a refractive index repartition.

Two parameters have been used to control the repartition. A first one characterizes the maximal value of the gradient $\mathbf{n_{plateau}}$ and a second one $\mathbf{G_{int}}$ characterizes the gradient intensity. Example of the refractive index distribution along the antero-posterior axis are given in the **[Figure 8.b]**

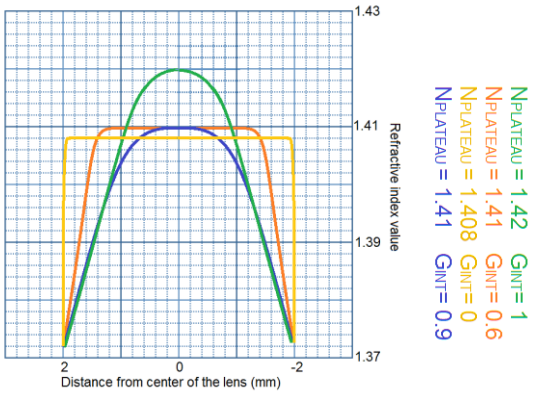

Figure 8.b: Examples of gradient intensity through the lens optical axis for different parameters couples.

After a first step of computation on the geometry with the **Wall Distance physics** the optical ray tracing can be performed using a definition of the refractive index value (in the material properties) with a function ***f*** of form described in **[Equation 1].**

$$n = f(n_{plateau}, G_{int}, wd.Dw, U)$$

Equation 1: refractive distribution function with the following variable: $\mathbf{n_{plateau}}$ **:** *Maximal refractive central value //* $\mathbf{G_{int}}$ **:** *gradient intensity //* **wd.Dw :** *vector of distance from the boundaries (normed in the function to obtain 0 at the periphery, 1 at the center) returned by the* ***Wall Distance physics*** *static step //* **U :** *displacement field*

Geometric preparations

We examine here the case of the eye of a young 22 Y.O. emmetropic healthy female patient. Imaging provided from an OCT (CASIA II, *Tomey*) have provided the geometry in the optical axis for two optical stimuli (0D – *far vision*, 6D - *near vision*). The axial length of the eye has been measured with an IOL Master 500 (*Zeiss*).
The eye is designed in the most accommodated shape (most relaxed geometry of the lens) and the posterior zonula is set in tension with a load ramping until the far vision thickness is achieved.
The material properties of the lens were age-dependant following the measurements of Wilde & Al **[1]**
The radii of curvature of the anterior/posterior lens surfaces, and the anterior chamber depth are compared with the far vision measurement, and some none measured parameter are adjusted as follow:
- The anterior and posterior zonular insertion on the capsule were manually tuned so that the ratio of the curvature radii change matches the far vision measurement.
- The axial position of the ciliary muscle was adjusted so that the displacement of the central anterior and posterior surface of the lens match the far vision measurement.
Once the unaccommodated geometry enters a tolerance of +/- 5% with the far vison measurement, the model is considered as ready.

Deduction of the refractive index distribution - Methodology

A. First we suppose that *the refractive index is homogeneous* in the lens.

a) The eye being considered emmetropic, the refractive index is computed for far vision. A **parametric sweep** of different refractive index is applied to find the one corresponding to the best focus on the retina in the far vision condition
b) Then this value is applied to the initial accommodated geometry (near vision), and a parametric sweep of light emission corresponding to different distance of object using a **release from grid** is applied. The distance corresponding to the best focus for this geometry is obtained this way.
c) A *second equivalent homogeneous refractive index* is computed in the same way as **a)** for a light emission corresponding to the near vision stimuli (6D) on the initial geometry (accommodated).

B. In a second time *we consider the model of the GRIN (Gradient of Refractive INdex)* detailed previously, and that a unique couple of two parameters for this GRIN can fit both visual conditions.

a) 2 variables parametric sweep considering the two GRIN parameters is applied to the near vision geometry with an optical light emission corresponding to 6D.
b) 2 variables parametric sweep considering the two GRIN parameters is applied to the far vision geometry with an optical light emission corresponding to 0D.
c) The couples of parameters close to match both vision conditions are extracted and the step **B.a)** and **B.b)** are repeated with a refined range of parametric sweep until a unique couple of parameter is found.

III. Results

Geometric Preparation

The **[Table 1]** shows the principal geometric results for the far vision simulated. The geometry obtained will be the one used in the rest of the tests.

Values	Expected	Simulated	%Difference
Thickness(mm)	3,440	3,440	0.00%
Ant. Curv. Radius (mm)	11,610	11,650	0,34%
Pos. Curv. Radius (mm)	6,240	6,400	2,56%
Ant/Pos. Disp. Ratio	0,810	0,805	0,62%

Table 1: *After a few geometric iterative adjustments of the initial geometry for non-measurable parameters, the far vision was obtained with geometric differences in the lens position/shape about less than 3%.*

A. Lens homogeneous refractive index hypothese

a) The refractive index corresponding to the best focus on the retina Far Vision has been found to be $\mathbf{n_{FV}}$ **= 1.436.**

b) When applied to the near vision this refractive index results in an amplitude of vision of **4.35 D**.

c) The refractive index corresponding to the best focus on the retina for near vision (6D) has be found to be $\mathbf{n_{NV}}$ **= 1.441**

The results of this phase show that we cannot find a unique refractive index (homogeneous) applied to the whole lens that matches the amplitude of the patient's stimuli (0-6D). It's coherent that, when the far vision refractive index induces an amplitude of 4.35D, the near vision refractive index needs to be significantly higher when computed for near vision.

B. Gradient of refractive index model

.
After 3 iterations of parametric sweep (ex: **[Figure 9]**) the couple of values giving best acuity for far and near vision (0-6D stimuli) was found: a plateau value of the refractive index of $\mathbf{n_{plateau}}$ **= 1.4175** and a coefficient characterizing the intensity of the gradient distribution of $\mathbf{G_{INT}}$ **= 0.95,** see **[Figure 10].**

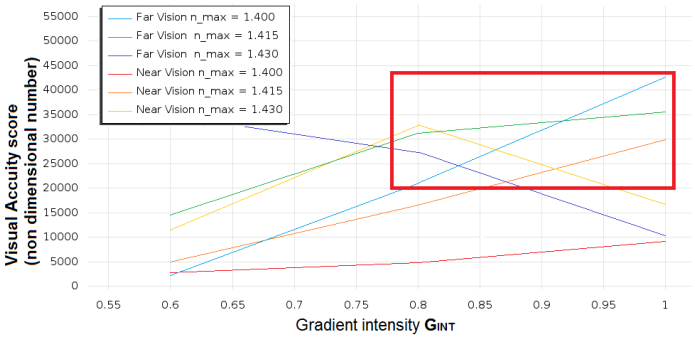

Figure 9: Parametric sweep of the score of acuity (no dimension) for sets of two variables *(color lines correspond to the plateau refractive index values, horizontal axis corresponds to the gradient intensity (no dimension))*. We can see that a matching couple of parameters fitting both near and far vision can be found by refining the red rectangle area *(values of* $n_{plateau}$ *between [1.415; 1.430] and values of* G_{INT} *between [0.8; 1])*.

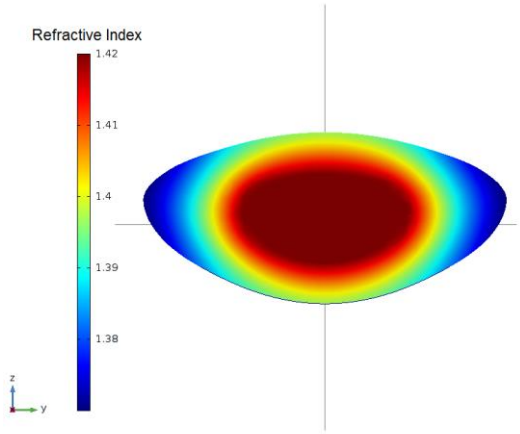

Figure 10: Map of the gradient of refractive index matching the two states of vision.

IV. DISCUSSION

Effect of the GRIN

The test A has shown that, to ensure a complete accommodation amplitude for the measured geometries, two equivalent refractive index values were needed with:
- Far vision: $\mathbf{n_{FV} = 1.436}$
- Near vision**:** $\mathbf{n_{NV} = 1.441}$

These values are completely in the range of the equivalent refractive index computed from measurements in the literature **[Figure 11]**.
The values in the literature are mainly computed with the application of simplified formulas to the measured geometries without considering the GRIN. The deduction of the refractive index can be performed in the far vision geometry (Ex: Dubbelman & Al.) or near vision (Ex: Atchinson & Al.).

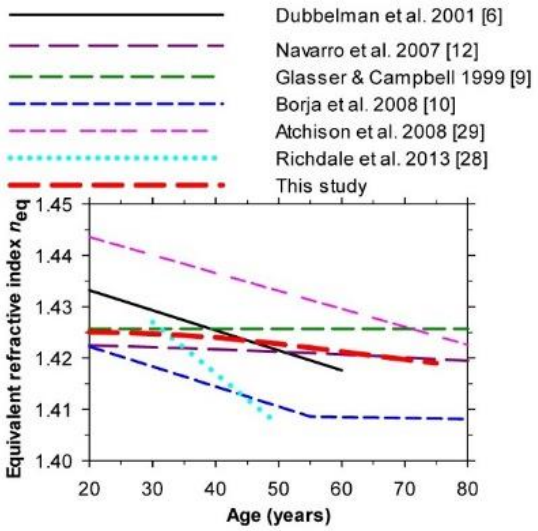

Figure 11: Equivalent refractive index measurement from different studies against age, extracted from **[8]**.

We have also found the couple of values for the GRIN model that fits both visual conditions. The value of the plateau is significantly lower than the values of the equivalent homogeneous values computed (***1.4175*** *for the plateau, versus* ***1.436 - 1.441*** *for the homogenous values*). The refractive power induced by the gradient distribution is higher, despite the absolute values of the refractive index being lower. This highlight an interesting structural design of Nature to maximize the optical power of this biological tissue. The **[Figure 12]** shows how, for a same maximal value of the plateau, the gradient intensity can induce important optical results.

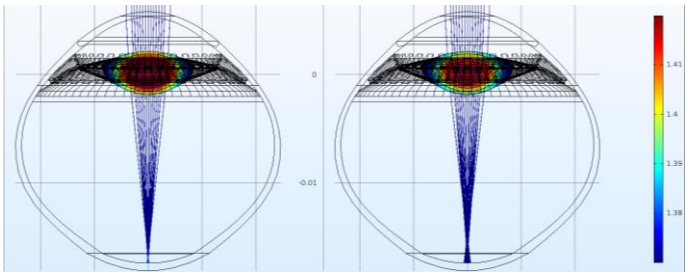

Figure 12: Effect of two different $\mathbf{G_{int}}$ parameters (same plateau value) in far vision. The gradient induces bigger changes that the maximal values.

The **[Figure 13]** is extracted on a study about the evolution of the GRIN with age.

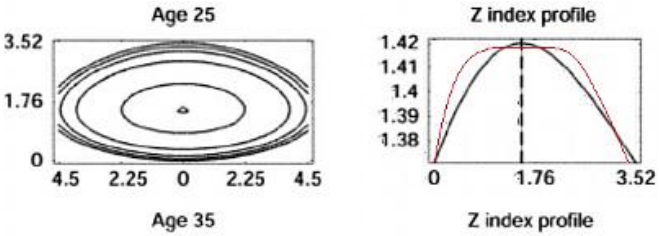

Figure 13: 25 Y.O. human lens GRIN contour measurement, from **[9].** We've superposed in red the values found for this model to the values of the publication.

Here the values computed from the model look really coherent with the measurements ($\mathbf{n_{plateau} = 1.4175}$ instead of **1.42**). The **[Figure 13]** display the GRIN profile in our model in red above measurement data from publication **[9]**.

The gradient of refractive index acts as a multiplicative factor for the accommodation: as the lens tissues (with their specific refractive index) move with the lens accommodation, it results in two different optical configurations for each extreme state. This interesting natural optical structure enables the eye to obtain a greater range of focus with lower maximal value of refractive index. A schematic drawing in **[Figure 14]** explains this phenomenon. Moreover, the GRIN increases the contrast and sharpness of the pictures on the retina by suppressing a lot of marginal rays and spherical aberrations of the eye optical system.

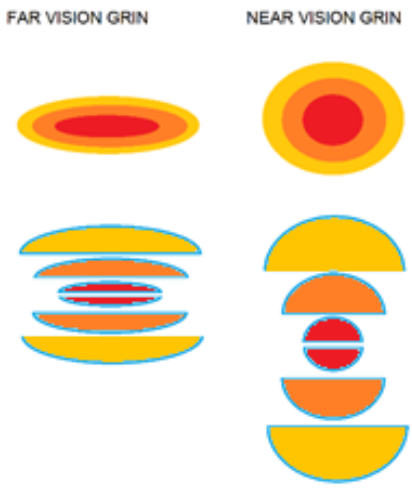

Figure 14: Simplified finite multilayer representation of the GRIN with decomposition in equivalent lens for each layer.

Biomimetic applications inspired by this process could be applied to optical systems needing wide range of focus in a compact format, such as – for instance- embedded camera or smartphones

V. CONCLUSION

The deduction of some not measured parameters has been performed using reverse engineering on a complete parametric model. The values obtained were coherent and highlight an interesting optical structure of the human lens.

This kind of model enables to understand more complex phenomena than models focusing only on the lens thanks to the optomechanical coupling. As today's medicine pays more and more attention to individualized solutions with the development of computational power and additive manufacturing for instance, the method developed here could be applied to other parameters such as mechanical properties to allow precise simulations of patient's eye for diagnosis, decision, surgery planning and/or solution.
The iterative methodology could also be integrated in further work in specific application using the **Application Builder** and the **Optimization Module** to provide ready to use tools for clinicians, who desire to access new parameters using a standard ophthalmologic equipment such as an OCT.

VI. REFERENCES

[1] c.-k. Chai, h.j. Burd, g.s. Wilde , "Shear modulus measurements on isolated human lens nuclei"
[2] Heather A. Anderson; Gloria Hentz; Adrian Glasser; Karla K. Stuebing; Ruth E. Manny, "Minus-Lens–Stimulated Accommodative Amplitude Decreases Sigmoidally with Age: A Study of Objectively Measured Accommodative Amplitudes from Age"
[3] Kaufman, *Adler's Physiology of the Eye - 11th*
[4] Allvar Gullstrand, "Nobel price lecture:"How I found the mechanism of intracapsular accommodation"", 1911
[5] M. Dubbelman, G.L. Van der Heijde, "The shape of the aging human lens: curvature, equivalent refractive index and the lens paradox"
[6] M. Dubbelman, G.L. Van der Heijde, H.A. Weeber , G.F.J.M. Vrensen "Changes in the internal structure of the human crystalline lens with age and accommodation"
[7] Sanjeev Kasthurirangan; Emma L. Markwell; David A. Atchison; James M. Pope, "In Vivo Study of Changes in Refractive Index Distribution in the Human Crystalline Lens with Age and Accommodation"
[8] W. Neil Charman and David A. Atchison "Age-dependence of the average and equivalent refractive indices of the crystalline lens"
[9] Díaz, José & Pizarro, Carles & Arasa, Jose. « Single dispersive gradient-index profile for the aging human lens". 2008
[10] Hung, George K., and John L. Semmlow. "Static behavior of accommodation and vergence: computer simulation of an interactive dual-feedback system." 1980
[11] Sun, F. U. C. H. U. A. N., and L. A. W. R. E. N. C. E. Stark. "Switching control of accommodation: experimental and simulation responses to ramp inputs." 1990
[12] Schor, Clifton M. "A dynamic model of cross-coupling between accommodation and convergence: simulations of step and frequency responses." 1992
[13] Hooker, R. J., et al. "Analog computer simulation of accommodation." Engineering in Medicine and Biology Society, 1996.
[14] Jouve, Francois, and Khalil Hanna.
"Computer Simulations of Refractive Surgery and Accommodation Mechanisms." 1999.
[15] Popiolek-Masajada, Agnieszka, and Henryk Kasprzak. "Model of the optical system of the human eye during accommodation." 2002
[16] Breitenfeld, P., T. Ripken, and H. Lubatschowski. "Finite element method-simulation of the human lens during accommodation." European Conference on Biomedical Optics 2005.
[17] Ljubimova, Darja. Numerical modelling of the human eye accommodation. Diss. 2005.
[18] Fink, Wolfgang, and Daniel Micol. "simEye: computer-based simulation of visual perception under various eye defects using Zernike polynomials." 2006
[19] Ljubimova, Darja, Anders Eriksson, and Svetlana Bauer. "Aspects of eye accommodation evaluated by finite elements." 2008
[20] Bocskai, Z. I. "Numerical simulation of the human eye accommodation." Proceedings of the Conference of Junior Researchers in Civil Engineering. 2012.
[21] Bocskai, Zoltán, and Imre Bojtár. "Biomechanical modelling of the accommodation problem of human eye." 2013